

# Quantum oscillations, colossal magnetoresistance, and the magnetoelastic interaction in bilayered $\text{Ca}_3\text{Ru}_2\text{O}_7$

G. Cao

*Department of Physics and Astronomy, University of Kentucky, Lexington, Kentucky 40506*

L. Balicas, Y. Xin, and J. E. Crow

*National High Magnetic Field Laboratory, Tallahassee, Florida 32310*

C. S. Nelson

*Department of Physics, Brookhaven National Laboratory, Upton, New York 11973*

(Received 24 December 2002; published 6 May 2003)

We report magnetic and interplane transport properties of  $\text{Ca}_3\text{Ru}_2\text{O}_7$  at high magnetic fields and low temperatures.  $\text{Ca}_3\text{Ru}_2\text{O}_7$  with a bilayered orthorhombic structure is a Mott-like system with a narrow charge gap of 0.1 eV. Of a host of unusual physical phenomena revealed in this study, a few are particularly intriguing: (1) a collapse of the  $c$ -axis lattice parameter at a metal-nonmetal transition,  $T_{MI}$  (= 48 K), and a rapid increase of  $T_{MI}$  with low uniaxial pressure applied along the  $c$  axis; (2) quantum oscillations in the gapped, nonmetallic state for  $20 \text{ mK} < T < 6.5 \text{ K}$ ; (3) tunneling colossal magnetoresistance, which yields a precipitate drop in resistivity by as much as 3 orders of magnitude; (4) different in-plane anisotropies of the colossal magnetoresistance and magnetization. All results appear to indicate a highly anisotropic ground state and a critical role of coupling between lattice and magnetism. The implication of these phenomena is discussed.

DOI: 10.1103/PhysRevB.67.184405

PACS number(s): 75.47.Gk, 72.15.Gd, 75.50.Ee

Layered ruthenium oxides or ruthenates as a new class of correlated electron systems are characterized by the coexistence of different kinds of order and various magnetic and electronic transitions that are generally abrupt and anisotropic. These materials have increasingly drawn attention in recent years,<sup>1</sup> but the  $4d$ -electron-based ruthenates are still by and large uncharted territory rich with novel physical phenomena that very often deviate from those of semiconductors, metals, or even  $3d$ -electron transition-metal oxides. Here the rich and intriguing physical properties observed in bilayered  $\text{Ca}_3\text{Ru}_2\text{O}_7$  provide another striking example that defies conventional notions.

$\text{Ca}_3\text{Ru}_2\text{O}_7$  is a recently discovered correlated electron system<sup>2</sup> that displays a low-temperature Mott “insulating” transition and possesses an unusually wide array of unique physical properties.<sup>2-7</sup> It is characterized by an exceptionally strong coupling of charge, spin, and lattice degrees of freedom along with numerous long-range magnetic ordered phases. The intra-atomic Coulomb interaction  $U$  is believed to be comparable to the kinetic energy or bandwidth  $W$ ; thus any small perturbations such as external magnetic fields can readily prompt drastic changes in the ground state. It is this competition between  $U$  and  $W$  that is at heart of the novel physical phenomena in  $\text{Ca}_3\text{Ru}_2\text{O}_7$ .

$\text{Ca}_3\text{Ru}_2\text{O}_7$  is known to undergo antiferromagnetic ordering at  $T_N = 56 \text{ K}$  followed by an abrupt metal-nonmetal transition at  $T_{MI} = 48 \text{ K}$  with a partial gapping of the Fermi surface.<sup>2,4,7</sup> Intermediate between  $T_N$  and  $T_{MI}$  there exists an antiferromagnetic metallic phase<sup>2</sup> (AFM), which itself is a rare occurrence for a stoichiometric or undoped compound at ambient pressure.<sup>8</sup>  $\text{Ca}_3\text{Ru}_2\text{O}_7$  also undergoes a first-order metamagnetic transition to a field-induced ferromagnetic metallic (FMM) phase at  $T < T_{MI}$  where spins are almost fully

polarized along the  $a$  axis, the easy axis for magnetization below 42 K, and concomitantly negative magnetoresistive.<sup>2,3</sup> The strong coupling among spin, charge, and lattice degrees of freedom in  $\text{Ca}_3\text{Ru}_2\text{O}_7$  is manifested as well in Raman studies,<sup>4,7</sup> where the Raman spectra reveal that the metal-nonmetal transition at  $T_{MI}$  is accompanied by a softening and broadening of an out-of-phase  $c$ -axis Ru-O phonon mode and a rapid suppression of low-frequency electronic scattering associated with the formation of a partial charge gap of  $\Delta_C \sim 0.1 \text{ eV}$ .<sup>4</sup> The corresponding gap ratio  $R = \Delta_C / k_B T_{MI} \sim 23$  is large, suggesting that the gap and thus  $T_{MI}$  are driven by strong electronic correlations, typical of a Mott-Hubbard system.<sup>9,10</sup> In addition, the optical conductivity of  $\text{Ca}_3\text{Ru}_2\text{O}_7$  yields a large scattering rate, leading to a remarkably short mean free path  $l$ , which is highly anisotropic, ranging from 0.8 to 8 Å, well beyond the limit for bandlike transport, or the Mott-Ioffe-Regel limit, assuming a typical Fermi velocity of  $10^7 - 10^8 \text{ cm/s}$ .<sup>5</sup>

In this paper, we report detailed magnetic and interplane transport properties primarily at high magnetic fields and low temperatures. Among a wide array of interesting physical phenomena, a few major observations seen in this study are highly unusual: (1) A collapse of the  $c$ -axis lattice parameter unexpectedly occurs at  $T_{MI}$ , which increases rapidly with low uniaxial pressure applied along the  $c$  axis. (2) A 90° rotation of the magnetic easy axis takes place in the vicinity of  $T_{MI}$  due to a drastic change in spin-orbital coupling through the lattice degree of freedom. (3) quantum oscillations (QO's) or the Shubnikov-de Haas (SdH) effect occurs in a state with a partial charge gap of 0.1 eV below  $T_{MI}$ .<sup>4</sup> The QO's with extremely low frequencies are observed in the  $c$  axis or interplane resistivity  $\rho_c$  for the magnetic field  $B$  parallel to the  $c$  axis at low temperatures. It is also found that

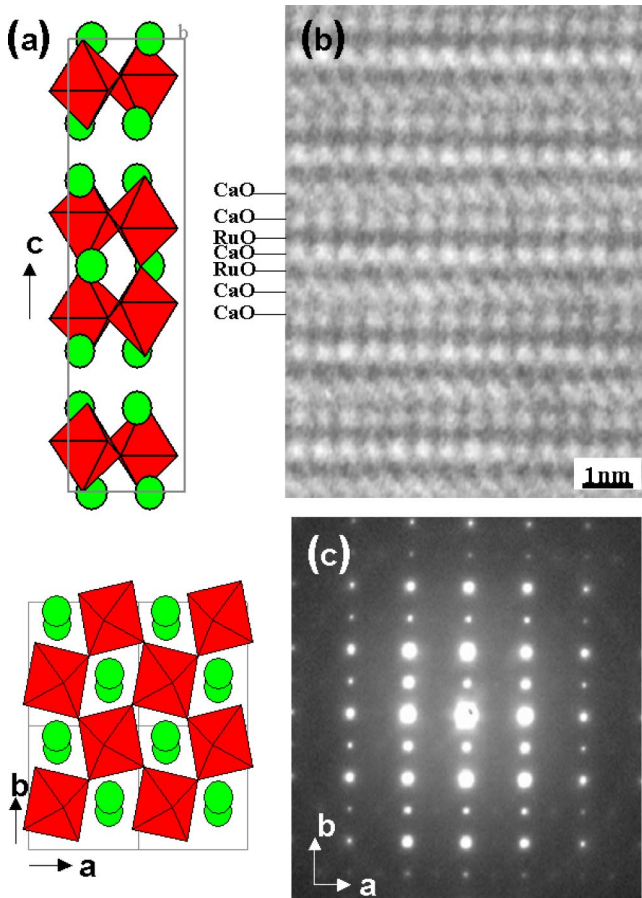


FIG. 1. (Color online) (a) Crystal structure of  $\text{Ca}_3\text{Ru}_2\text{O}_7$ . (b) The TEM image along the  $[010]$  zone axis. (c) The diffraction pattern of the basal plane.

the QO's reoccur with a higher frequency when  $B$  is higher than the metamagnetic transition and within the  $ac$  plane. (4) When  $\mathbf{B}$  is parallel to the  $a$  or  $b$  axis, the interplane resistivity  $\rho_c$  exhibits tunneling magnetoresistivity, which yields a precipitous drop in resistivity by as much as three orders of magnitude. (5) However, the decrease in  $\rho_c$ , or the interplane negative magnetoresistivity for  $B \parallel b$  axis, the hard axis, is two orders of magnitude larger than that for  $B \parallel a$  axis, the easy axis, where the magnetization is fully polarized at  $B > 6 \text{ T}$ .<sup>2</sup> All these results point toward the critical role of structural distortion and the coupling between lattice and magnetism through the orbital degree of freedom, which primarily drive the rich physical phenomena.

With a double Ru-O layered orthorhombic structure,<sup>3</sup>  $\text{Ca}_3\text{Ru}_2\text{O}_7$  belongs to the Ruddlesden-Popper series,  $\text{Ca}_{n+1}\text{Ru}_n\text{O}_{3n+1}$ , with  $n=2$ , where  $n$  is the number of coupled Ru-O layers in a unit cell, as shown in Fig. 1(a). It has a  $B2_1ma$  space group (or  $Cmc2_1$  with the  $a$  axis being the long axis) and lattice parameters of  $a=5.3720(6) \text{ \AA}$ ,  $b=5.5305(6) \text{ \AA}$ , and  $c=19.572(2) \text{ \AA}$ .<sup>3</sup> The layered nature is clearly illustrated in the transmission electron microscopy (TEM) image along the  $[010]$  zone axis [see Fig. 1(b)], where the stacking sequence of Ru-O and Ca-O layers is visible. The crystal structure is severely distorted by rotations and tilting of  $\text{RuO}_6$  (for details see Ref. 3). The struc-

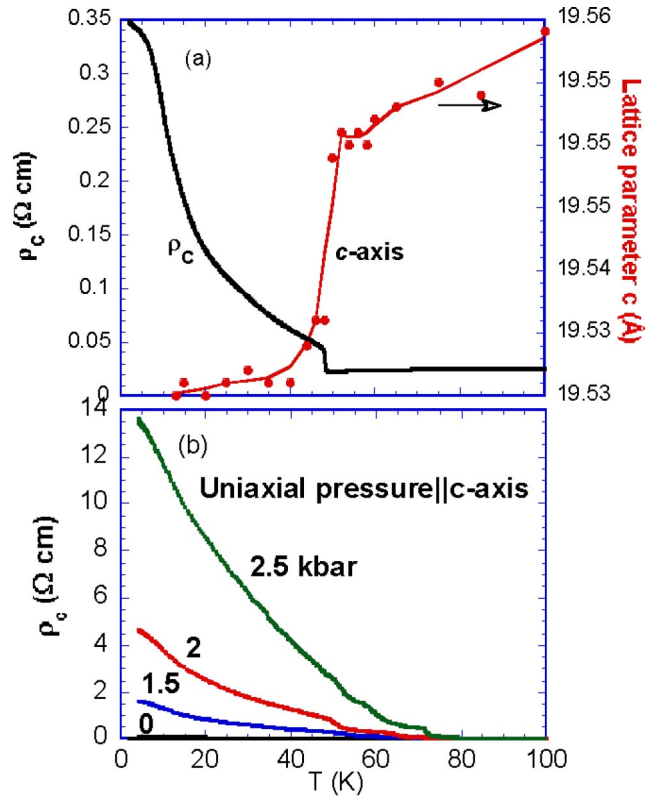


FIG. 2. (Color online) (a) Resistivity  $\rho_c$  (left scale) and the  $c$ -axis lattice parameter as a function of temperature  $T$ . (b)  $\rho_c$  vs  $T$  at low uniaxial pressures: 0, 1.5, 2, 2.5 kbar.

tural anisotropy in basal planes is noticeably reflected in the diffraction pattern shown in Fig. 1(c) where extra spots due to a dynamic effect are visible along the  $b$  axis. As can be seen below, this anisotropy results in a highly anisotropic ground state when  $\mathbf{B}$  is parallel to the  $a$  or  $b$  axis.

Shown in Fig. 2(a) are the  $c$  axis or interplane resistivity  $\rho_c$  and the lattice parameter for the  $c$  axis (right scale) as a function of temperature. The data obtained from x-ray diffraction reveal a rapid decrease in the  $c$  axis at  $T_{MI}$ , but no systematic changes in the  $ab$  plane (it is not yet clear if the structural symmetry remains unchanged). The simultaneous structural, electronic, and magnetic transitions at  $T_{MI}$  unambiguously indicate a magnetoelastic effect, a major characteristic of  $\text{Ca}_3\text{Ru}_2\text{O}_7$ , which is also seen in the Raman study.<sup>4,7</sup> It seems surprising that the collapse of the  $c$  axis lattice parameter, which would be expected to enhance the interplane orbital overlapping, does not lead to a more metallic state, but conversely, a partial gapping of the Fermi surface and nonmetallic ground state. This is evidenced by an abrupt metal-nonmetal transition at  $T_{MI}=48 \text{ K}$  followed by a rapid increase in  $\rho_c$  by as much as a factor of 18. It is likely that the collapse of the  $c$ -axis lattice parameter may be associated with a Jahn-Teller-like distortion of the Ru-O octahedra, which lifts the degeneracy of the  $t_{2g}$  orbitals by lowering the energy of the  $d_{xy}$  orbital relative to that of the  $d_{yz}$  and  $d_{xz}$  orbitals.

Recent first-principles calculations for  $\text{Sr}_2\text{RuO}_4$  indicate that the shortening of the  $c$  axis or the flattening of  $\text{RuO}_6$ ,

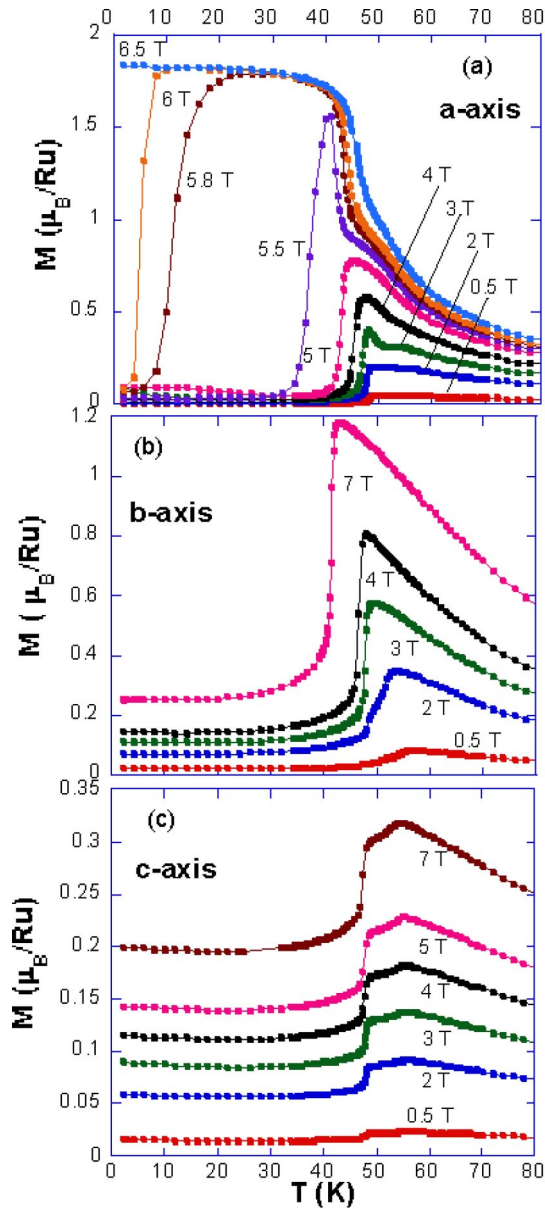


FIG. 3. (Color online) Magnetization  $M$  as a function of  $T$  for (a) the  $a$  axis, (b) the  $b$  axis, and (c) the  $c$  axis at various magnetic fields.

which results in orbital polarization and reducing bands of three  $t_{2g}$  states, is the key fact to stabilize the insulating magnetic ground state.<sup>11</sup> This point may also be valid for  $\text{Ca}_3\text{Ru}_2\text{O}_7$ . As can be seen in Fig. 2(b), both  $T_{MI}$  and the magnitude of  $\rho_c$  rise drastically even at low uniaxial pressure applied along the  $c$  axis, for instance, at 2.5 kbar,  $T_{MI}$  increases to 73 K and  $\rho_c$  jumps by more than 2 orders of magnitude. In contrast, the uniaxial stress along the  $a$  axis and hydrostatic pressure leads to a decrease in  $T_{MI}$  and resistivity,<sup>12</sup> consistent with the recent Raman results.<sup>7</sup>

Figure 3 shows the longitudinal magnetization,  $M(T)$ , as a function of temperature  $T$  for all three principal crystallographic axes at different magnetic fields  $B$ . Along the  $a$  axis [Fig. 3(a)],  $M(T)$  features two phase transition temperatures,  $T_N=56$  K and  $T_{MI}=48$ , as reported earlier.<sup>2,3</sup>  $M$  drops pre-

cipitously below  $T_{MI}$ , indicating a magnetoelastic effect occurring upon the collapse of the  $c$ -axis lattice parameter shown in Fig. 2(a). The  $a$  axis is apparently the easy axis for magnetization for  $T < 42$  K (as discussed below, the easy axis rotates to the  $b$  axis for  $42 \text{ K} < T < T_N$ ) since  $M(T)$  is lowest along this direction for the antiferromagnetic state. As  $B$  increases,  $T_{MI}$  shifts slightly, whereas  $T_N$  remains essentially unchanged initially and becomes rounded eventually. At  $B = 6$  T, the magnetic ground state becomes ferromagnetic, consistent with isothermal magnetization where the system undergoes the first-order metamagnetic transition to the ferromagnetic state with nearly fully polarized spins (saturation moment,  $M_0 > 1.73 \mu_B/\text{Ru}$ ), suggesting more than 85% spin polarization, assuming  $2 \mu_B/\text{Ru}$  expected for an  $S=1$  system. The metamagnetic transition along the  $b$  and  $c$  axes is much broader and occurs at much higher fields.<sup>2,3</sup>

It is worth mentioning that given such a relatively low metamagnetic transition field along the  $a$  axis, it is legitimate to speculate that below 42 K spins along the  $a$  axis are *ferromagnetically and strongly* coupled within bilayers that are, however, *antiferromagnetically and weakly* coupled along the  $c$  axis, i.e., between bilayers. The weak antiferromagnetic coupling between the neighboring bilayers is reflected by the fact that only 6 T is needed to drive the metamagnetic transition and flip the spins. Shown in Fig. 3(b) is  $M(T)$  for the  $b$  axis, which exhibits no anomaly corresponding to  $T_{MI}$  but a much stronger peak at  $T_N$ . Unlike  $T_N$  for the  $a$  axis,  $T_N$  for the  $b$  axis decreases as  $B$  increases. The magnetic ground state remains antiferromagnetic.  $M(T)$  for the  $c$  axis displays the two transitions, which, however, are largely weakened and yet insensitive to  $B$  [Fig. 3(c)]. The different trends along the different axes suggest highly anisotropic magnetic exchange coupling that is coupled with the lattice degree of freedom.

Such a large magnetocrystalline anisotropy also leads to an anomalous angular dependence of  $M$ . Shown in Fig. 4 is  $M(B=6.2 \text{ T})$  as a function of angle  $\Theta$ , defined as the angle between  $B$  and the easy axis, i.e., the  $a$  axis. Unlike magnetization of ordinary ferromagnets such as  $\text{CrO}_2$  and  $\text{SrRuO}_3$  where uniaxial magnetocrystalline anisotropy gives rise to a simple angular dependence described by  $M = M_S \cos \Theta$ ,  $M$  for  $\text{Ca}_3\text{Ru}_2\text{O}_7$  changes abruptly with  $\Theta$  and shows no simple behavior similar to  $M = M_S \cos \Theta$ . For  $T < 42$  K,  $M$  saturates at  $1.73 \mu_B/\text{Ru}$  at  $\Theta = 0^\circ$ , i.e., along the  $a$  axis, and precipitously drops as  $\Theta$  increases and becomes  $0.07 \mu_B/\text{Ru}$  at  $\Theta = 40^\circ$ . As  $\Theta$  further increases, a broad peak appears around  $\Theta = 90^\circ$ , i.e., the  $b$  axis. When  $T > 42$  K, the angular dependence of  $M$  changes drastically as seen in Figs. 4(a) and 4(b). Apparently, the easy axis starts to rotate away from the  $a$  axis at 42 K and finally becomes parallel to the  $b$  axis at 55 K where the angular dependence follows a simple cosinelike behavior.

It is noted that at 55 K where the system becomes much more itinerant, the magnetization along the  $b$  axis is  $0.8 \mu_B/\text{Ru}$ , only about a half of the saturation moment when the easy axis is parallel to the  $a$  axis. The reduction of the saturation moment could be due to the presence of the metallic state where electrons are expected to be much less localized than those below  $T_{MI}$  but the gapping, which is driven by electron correlations, may not be reflected in the

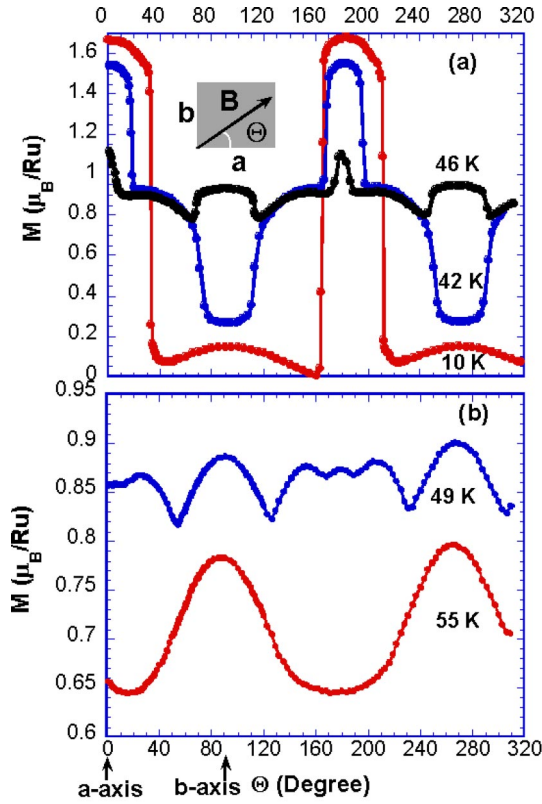


FIG. 4. (Color online)  $M$  at  $B = 6.2$  T as a function of angle  $\Theta$  defined as the angle between  $B$  and the easy axis, i.e., the  $a$  axis for (a)  $T = 10, 42,$  and  $46$  K and (b)  $T = 49$  and  $56$  K.

spatial behavior of the wave functions. Nevertheless, since the magnetocrystalline anisotropy is due mainly to spin-orbit coupling through lattice, the rotation of the easy axis or the change of anisotropy clearly indicates a drastic change in the spin-orbit coupling that is closely associated with the collapse of the  $c$ -axis lattice parameter or the magnetoelastic interaction. These results along with the data shown in Fig. 2 suggest that the nonmetallic antiferromagnetic state below  $T_{MI}$  may be indeed driven by the flattening of  $\text{RuO}_6$  and the coupling of orbital and lattice degrees of freedom, as suggested in Ref. 11.

Remarkably, the angular dependence of resistivity perfectly mirrors that of magnetization. Shown in Fig. 5 is the angular dependence of  $\rho_c$  and  $M$  for  $B (= 6.2$  T) rotating in the  $ac$  plane at low temperatures. While  $M$  behaves in the same fashion as that for  $B$  rotating in the  $ab$  plane, the mirrored angular dependence of  $\rho_c$  ( $B = 6.2$  T) confirms the unusually strong spin-charge coupling: an abrupt drop (rise) in  $M$  immediately leads to a precipitous rise (drop) in  $\rho_c$  by more than an order of magnitude. The spin-charge coupling is even seen at  $20^\circ < \Theta < 160^\circ$  where a weak and broad peak of  $M$  vs  $\Theta$  results in a shallow and broad valley of  $\rho_c$ .

Indeed, the strong and complex coupling among spin, charge, orbit, and lattice gives rise to highly anisotropic magnetic and electronic properties for different principal crystallographic directions. These are further demonstrated in the interplane resistivity  $\rho_c$  with  $B$  parallel to the  $a$ ,  $b$ , and  $c$  axes, presented below.

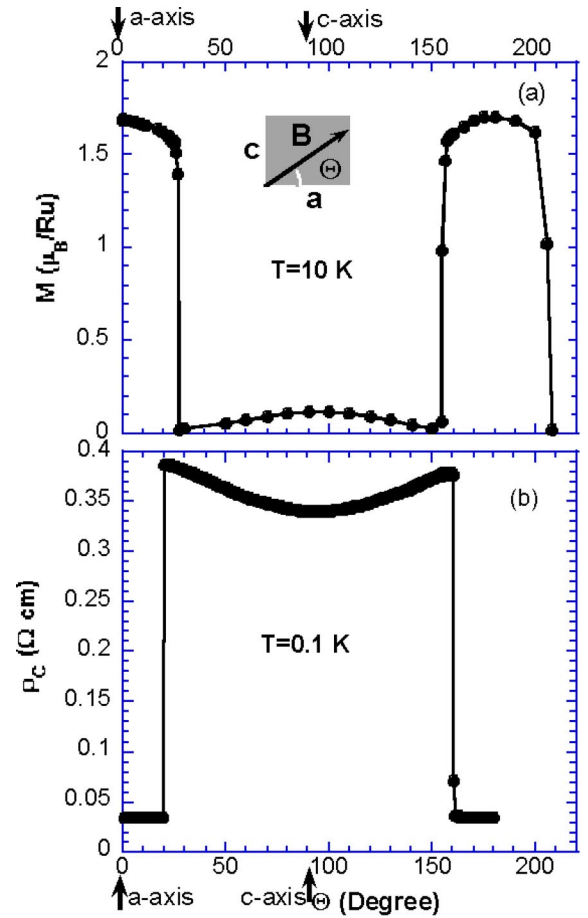


FIG. 5. The angular dependence of (a)  $M$  and (b)  $\rho_c$  at  $B = 6.2$  T for  $B$  rotating in the  $ac$  plane at low temperatures.

Figure 6(a) shows  $\rho_c$  as a function of  $B$  for temperatures ranging from 0.6 to 6.5 K as indicated.  $B$  is applied parallel to the interplane  $c$  axis. An oscillatory component, i.e., the SdH effect is developed as temperature decreases. The SdH oscillations at lower fields are shown in the inset for  $T = 20$  mK in a limited field range of  $2 < B < 12$  T. Shown in Fig. 6(b) is the amplitude of the SdH oscillations as a function of inverse field  $B^{-1}$  for several values of temperatures. The SdH signal is defined as  $(\sigma - \sigma_b)/\sigma_b$  where  $\sigma$  is the conductivity (or the inverse of  $\rho_c$ ) and  $\sigma_b$  is the background conductivity.  $\sigma_b$  is obtained by inverting the background resistivity, which is achieved by fitting the actual  $\rho_c$  to a polynomial. The inset shows the amplitude of the SdH signal normalized by temperature in a logarithmic scale. The solid line is a fit to the Lifshitz-Kosevich formulas,  $x/\sinh x$ , where  $x = 14.69m_cT/B$ . The fit yields a cyclotron effective mass  $m_c = 0.85 \pm 0.05$ . Markedly, this cyclotronic effective mass is different from the enhanced thermodynamic effective mass estimated from the electronic contribution,  $\gamma$ , to the specific heat.

This apparent disagreement between the thermodynamic effective mass and the cyclotronic effective mass is quite common in heavy-fermion systems<sup>13</sup> and is attributed to the fact that it has been difficult to resolve the higher effective masses in quantum oscillation experiments. It is clear that

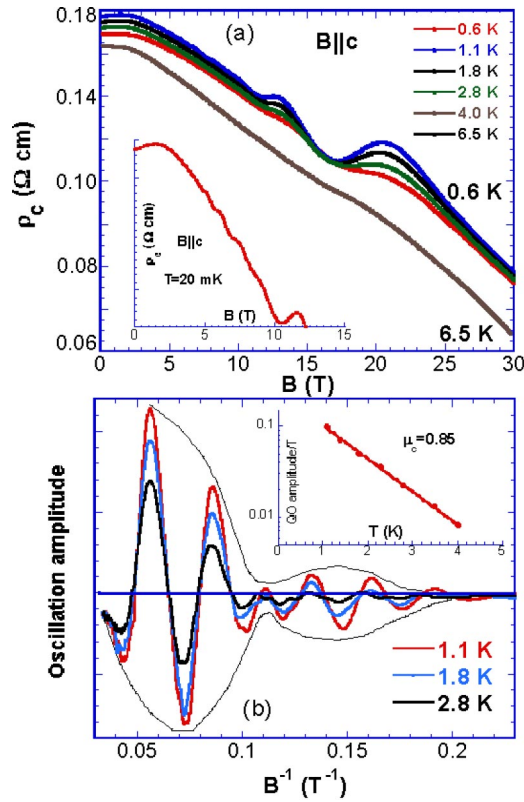


FIG. 6. (Color online) (a)  $\rho_c$  as a function of  $B$  for temperature ranging from 0.6 to 6.5 K as indicated for  $\mathbf{B}\parallel c$  axis; (b) the amplitude of the SdH oscillations as a function of inverse field  $B^{-1}$  for various temperatures. Inset: the amplitude of the SdH signal normalized by  $T$  in a logarithmic scale.

some portion of the Fermi surface with larger masses might have not been detected in our measurements. In addition, the SdH effect is conspicuously absent in resistivity for the  $a$  and  $b$  axes when  $\mathbf{B}\parallel c$ .

As clearly seen in Fig. 6(b), the detected frequencies are extremely low, and only a few oscillations are observed in the entire field range up to 45 T (above 25 T, no QO's are observed). Because of the limited number of oscillations, the usual fast-Fourier-transform analysis becomes unreliable in the present case. The frequencies can, however, be determined by directly measuring the period of the oscillations, for example, for  $B^{-1} \leq 0.1 \text{ T}^{-1}$ . This analysis reveals two frequencies visible in Fig. 6(b), the higher frequency of 28 T and the very low frequency of 10 T. The higher frequency of  $F_1 = 28 \text{ T}$ , based on crystallographic data of  $\text{Ca}_3\text{Ru}_2\text{O}_7$  (Ref. 3) and the Onsager relation  $F_0 = A(h/4\pi^2e)$  ( $e$  is the electron charge), corresponds to an area of only 0.2% of the first Brillouin zone (FBZ). In contrast, for all compounds studied so far, the de Haas-van Alphen (dHvA) frequencies range typically from hundreds to several thousand teslas. Small orbits in  $k$  space imply large orbits in real space or in a much lower probability of circling the entire Fermi-surface sheet due to any possible sources of scattering. For this reason, small orbits or low frequencies are much more difficult to be detected than higher ones, that is to say, one always detects high frequencies relatively easily and lower frequencies with more efforts, if any, in conventional metals. The exception-

ally low frequencies observed in this system are apparently intrinsic. It needs to be pointed out that the disappearance of the oscillations at  $B > 25 \text{ T}$  may indicate the proximity of the quantum limit [when the quantized magnetic energy  $\mathcal{E} = (n + \frac{1}{2})h\epsilon B/2\pi mc$  with  $n=0$  becomes comparable to the electronic or Fermi energy], which therefore imposes limitations on the applicability of the Lifshitz-Kosevich formalism<sup>14,15</sup> to the data presented here. The envelope of the SdH oscillations outlined by the dotted line shown in Fig. 6(b) suggests beating between the two close frequencies ( $F_2 \sim 10 \text{ T}$ ) and a possibly warped Fermi surface. Both frequencies are likely to correspond to neck and belly orbits, respectively.

It is known that QO's are commonly observed in organic compounds and many pure metals due to the generally high purity of these materials where weak electron scattering preserves the sharpness of Landau levels. It is in general more difficult to investigate QO's in alloys and oxides where structural defects, disorder, impurities, or large electron scattering inevitably broaden Landau levels and lead to a dampening of QO's. The occurrence of QO's in a partially gapped nonmetallic oxide such as  $\text{Ca}_3\text{Ru}_2\text{O}_7$  (Ref. 16) would be unlikely based on conventional physics that requires the existence of a Fermi surface (a metallic state) and a long mean free path ( $> 10^3 \text{ \AA}$ ) for QO's to occur. It may be plausible that the apparent contradiction of observing the QO's in the nonmetallic state may be attributed to very small Fermi-surface (FS) pockets resulting from the Fermi-surface reconstruction at  $T_{MI}$ . This occurs due to octahedral distortions discussed above and/or a spin-orbital ordering, i.e., a gap opens along most of the Fermi surface, leaving small reconstructed electron or hole pockets responsible for QO's. It is noted that orbital ordering is predicted to occur in single layered  $\text{Ca}_2\text{RuO}_4$  (Ref. 17) where a sudden change in the basal plane at  $T = 357 \text{ K}$  may be associated with orbital ordering.<sup>18,19</sup> For  $\text{Ca}_3\text{Ru}_2\text{O}_7$ , however, no similar changes in the  $a$  or  $b$  axes are discerned in spite of the collapse of the  $c$ -axis lattice parameter at  $T_{MI}$  discussed above (see Fig. 2).

The collapse of the  $c$ -axis lattice parameter may favor orbital polarization,<sup>11</sup> which, in turn, could alter the small Fermi surface facilitating the QO's. In addition, a highly inhomogeneous picture involving the coexistence of large metallic and insulating clusters has been widely discussed recently for manganites.<sup>20</sup> Within this framework, it could be speculated that SdH oscillations might occur within the metallic islands and that the insulating clusters might cause overall bad metallicity. However, the size of the orbits in real space, based on the Fermi surface estimated above, would be of the order of  $1000 \text{ \AA}$ , which means the metallic clusters need to be on a near-macroscopic scale.

Furthermore, no QO's have ever been reported in the manganites. Should the metallic islands be responsible for the QO's, the QO's would become even stronger when the metallic state is fully recovered at high magnetic fields. As seen below, the QO's are only seen in the partially recovered metallic state but not in the fully recovered metallic state, suggesting that the QO's may be unique to the nonmetallic state. The QO's in  $\text{Ca}_3\text{Ru}_2\text{O}_7$  may arguably manifest an exotic ground state, the understanding of which may require unconventional approaches and ideas.

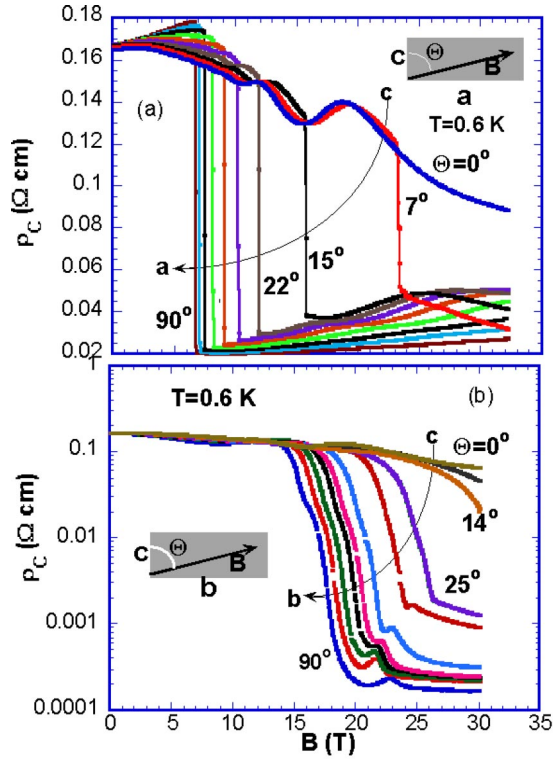


FIG. 7. (Color online)  $\rho_c$  as a function of  $B$  for various angles in (a) the  $ac$  plane at  $T=0.6$  K for  $0 \leq B \leq 30$  T and (b) the  $bc$  plane at  $T=0.6$  K for  $0 \leq B \leq 33$  T. Note that the angular dependence of the transition seem to track the sine function.

Shown in Fig. 7 is  $\rho_c$  as a function of  $B$  for various angles in (a) the  $ac$  plane at  $T=0.6$  K for  $0 \leq B \leq 30$  T and (b) the  $bc$  plane at  $T=0.6$  K for  $0 \leq B \leq 33$  T. For  $B$  within the  $ac$  plane, as  $B$  rotates away from the  $c$  axis, the SdH effect is overpowered by a precipitous drop in  $\rho_c$  or a first-order metamagnetic transition to a much more metallic state starting at  $\Theta = 15^\circ$ , where  $\Theta$  is defined as the angle between the  $c$  axis and  $B$  [see Fig. 7(a)]. The critical field  $B_c$  at which the metamagnetic transition occurs decreases as  $\Theta$  decreases or as  $B$  becomes more parallel to the  $a$  axis, along which spins are fully polarized at  $B=6$  T. When  $\Theta > 30^\circ$ , the SdH effect disappears completely below  $B_c$ . At  $\Theta=90^\circ$ , or  $\mathbf{B} \parallel a$ , the interplane magnetoresistivity ratio defined as  $\Delta\rho_c/\rho_c(0)$  is more than 91%, much larger than the  $a$ -axis magnetoresistivity ratio for  $\mathbf{B} \parallel a$ , i.e.,  $\Delta\rho_a/\rho_a(0)=60\%$ .<sup>21</sup> The larger interplane magnetoresistance is believed to be due to a tunneling effect facilitated by a field-induced coherent motion of spin-polarized electrons between Ru-O planes.

Because of the layered nature, the spin-polarized Ru-O planes sandwiched between insulating ( $I$ ) rocksalt Ca-O planes form a array of FM//FM junctions engineered by nature that largely enhance the probability of tunneling and thus electronic conductivity, which depends on the angle between the moments of adjacent ferromagnets.<sup>22</sup> Remarkably, when  $B > B_c$  and for  $20^\circ < \Theta < 60^\circ$ , the oscillations reoccur, showing a larger frequency of 47 T (see Fig. 8 for clarity), suggesting a possible restructured Fermi surface after the first-order metamagnetic transition.

The reoccurrence of the QO's with the larger frequency is

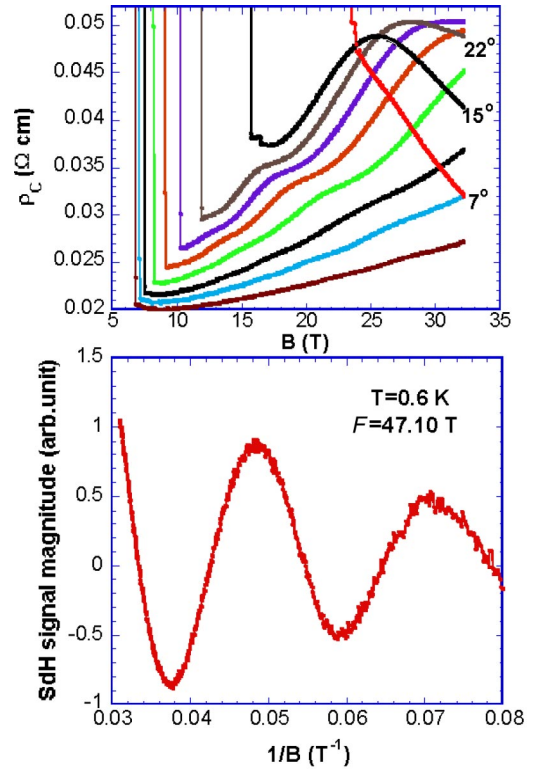


FIG. 8. (Color online) Enlarged  $\rho_c$  as a function of  $B$  for various angles in the  $ac$  plane at  $T=0.6$  K (upper panel). Amplitude of the SdH oscillations as a function of inverse field  $B^{-1}$  for  $B > B_c$  and  $\Theta=27^\circ$  (lower panel).

consistent with the view that the QO's are likely due to the small Fermi-surface pockets discussed above. However, this behavior is not seen in a more metallic state when  $B$  is within the  $bc$  plane as shown below. It is noted that the heavy-mass part of the Fermi surface, which contributes to the large  $\gamma$ , does not change at the metamagnetic transition, i.e.,  $\gamma$  is the same above and below the metamagnetic transition.<sup>23</sup> Shown in Fig. 7(b) is  $\rho_c$  (in logarithmic scale) as a function of  $B$  for various angles in the  $bc$  plane at  $T=0.6$  K for  $0 \leq B \leq 30$  T.  $\rho_c$  for  $B$  in the  $bc$  plane behaves similarly to  $\rho_c$  for  $B$  in the  $ac$  plane, but distinct features are apparent, among them, three are remarkable: (1) The metamagnetic transitions for  $B$  in the  $ac$  plane are first-order transitions with a large hysteresis, whereas the transitions for  $B$  in the  $bc$  plane are not only broader but also much higher than those for  $B$  in the  $ac$  plane seen in Fig. 7(a). (2) For  $B$  in the  $ac$  plane, oscillations reoccur when  $B > B_c$ , yielding a frequency of 47 T as discussed above and clearly shown in Fig. 8. In contrast, no oscillations are discerned for  $B$  in the  $bc$  plane even though  $\rho_c$  in this configuration is smaller by as much as 2 orders of magnitude than that for  $B$  in  $ac$  plane. The difference may suggest a critical role of the first-order metamagnetic transitions for  $B$  in the  $ac$  plane, which could largely alter the Fermi surface in favor of the reoccurrence of the QO's. (3) The drop in  $\rho_c$  for  $\mathbf{B} \parallel a$ , the easy axis, is 2 orders of magnitude smaller than that for  $\mathbf{B} \parallel b$ , the hard axis, completely contrary to the anisotropy of magnetization.<sup>3,21</sup> At lowest temperatures,  $\rho_c(0)/\rho_c(30 \text{ T}) \sim 10$  and  $10^3$  for  $\mathbf{B} \parallel a$  and  $\mathbf{B} \parallel b$ ,

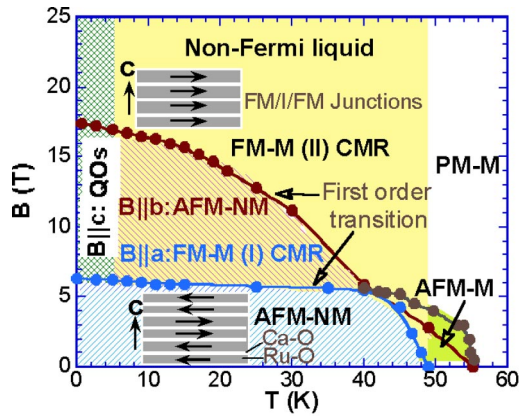


FIG. 9. (Color online)  $B$ - $T$  phase diagram summarizes major characteristics of  $\text{Ca}_3\text{Ru}_2\text{O}_7$  when  $\mathbf{B}$  is parallel to the  $a$ ,  $b$ , and  $c$  axis, respectively.

respectively. If the reduction of  $\rho_c$  seen here is chiefly driven by the spin polarization, then it is intriguing that  $\rho_c$  becomes so drastically smaller when  $\mathbf{B}$  is parallel to the hard axis  $b$  below 42 K. The spin-orbit interaction, which lowers the symmetry of atomic wave functions and mixes states, could lead to anisotropic scattering and thus anisotropic magnetoresistance. But anisotropic magnetoresistive effects are known to be small in general. Nevertheless, the different anisotropies for magnetization and resistivity clearly points out that *spin polarization alone cannot account for the colossal magnetoresistance and its large anisotropy observed here.*

A  $B$ - $T$  phase diagram shown in Fig. 9 summarizes major characteristics of  $\text{Ca}_3\text{Ru}_2\text{O}_7$  when  $\mathbf{B}$  is parallel to the  $a$ ,  $b$ , and  $c$  axes, respectively. The large anisotropy as a main feature is clearly shown. When  $\mathbf{B}||a$  axis, the easy axis, below 42 K, the colossal magnetoresistance or the ferromagnetic metallic state (I) [FM- $M$ (I)] is induced via the first-order metamagnetic transition at  $B = 6$  T, which is nearly temperature independent below 42 K. When  $\mathbf{B}||b$  axis or the hard axis below 42 K, the ferromagnetic metallic state (II) [FM- $M$ (II)] with two orders of magnitude larger conductivity is generated via the sharp transition that is strongly temperature dependent. When  $\mathbf{B}||c$  axis (shaded area), the QO's occur in the gapped nonmetallic state, persisting up to 6 K.

All results presented here repeatedly suggest an unusually strong coupling among spin, charge, and orbit through the lattice degree of freedom that governs the ground state. This characteristic is also reflected in recent theoretical studies. As mentioned above, the theoretical analysis based on the multi-orbital Hubbard model coupled to lattice distortions predicts orbital ordering and large magnetoresistance in the ruthenates.<sup>17</sup> A phase diagram generated from this theoretical analysis suggests a potential competition between metallic FM and insulating AFM states. Since the two-phase competition is a key concept to understand colossal magnetoresistance in manganites,<sup>22</sup> the colossal magnetoresistance is also predicted to occur in the ruthenates.<sup>17</sup> In addition, the first-principles calculations indicate that the flattening of  $\text{RuO}_6$  octahedra, or more generally, structural distortions, are critical in determining the ground state in  $\text{Sr}_2\text{RuO}_4$ .<sup>11</sup> This point seems to be also applicable in  $\text{Ca}_3\text{Ru}_2\text{O}_7$  where the critical role of the  $c$ -axis shortening for the presence of the AFM nonmetallic ground state is so evident. This is consistent with the results of the recent Raman study that also illustrates the important role of  $\text{RuO}_6$  octahedral flattening in stabilizing the AFM state in  $\text{Ca}_3\text{Ru}_2\text{O}_7$ .<sup>7</sup> It is remarkable that the different kinds of ordering, which are conventionally expected to exclude each other, seem to be characteristically synergistic in  $\text{Ca}_3\text{Ru}_2\text{O}_7$ . The extraordinary coexistence of both the nonmetallic and fermion-quasiparticle characteristics is intriguing and calls for innovative theoretical approaches to the extended, correlated electrons; the drastically different anisotropies of the colossal magnetoresistance and the magnetization signal an unusual scattering mechanism other than the spin-scattering dominated mechanism that works marvelously well in other materials. To address these profound new problems will surely broaden and deepen our understanding of fundamentals of correlated electrons in general and the ruthenates in particular.

G.C. would like to thank Dr. Elbio Dagotto, Dr. Daniel Agterberg, and Dr. David Singh for very useful discussions. Y.X. was supported by NHMFL under Cooperative Agreement DMR-0084173. The microscopy facilities were supported by Magnet Science and Technology Division at NHMFL.

<sup>1</sup>See, for instance, Y. Maeno, T. M. Rice, and M. Sigrist, *Phys. Today* **54** (1), 42 (2001).

<sup>2</sup>G. Cao, S. McCall, J. E. Crow, and R. P. Guertin, *Phys. Rev. Lett.* **78**, 1751 (1997).

<sup>3</sup>G. Cao, K. Abboud, S. McCall, J. E. Crow, and R. P. Guertin, *Phys. Rev. B* **62**, 998 (2000).

<sup>4</sup>H. L. Liu, S. Yoon, S. L. Cooper, G. Cao, and J. E. Crow, *Phys. Rev. B* **60**, R6980 (1999).

<sup>5</sup>A. V. Puchkov, M. C. Schabel, D. N. Basov, T. Startseva, G. Cao, T. Timusk, and Z.-X. Shen, *Phys. Rev. Lett.* **81**, 2747 (1998).

<sup>6</sup>R. P. Guertin, J. Bolivar, G. Cao, S. McCall, and J. E. Crow, *Solid State Commun.* **107**, 263 (1998).

<sup>7</sup>C. S. Snow, S. L. Cooper, G. Cao, J. E. Crow, S. Nakatsuji, and Y. Maeno, *Phys. Rev. Lett.* **89**, 226401 (2002).

<sup>8</sup>In the phase diagrams of  $\text{NiS}_{1-x}\text{Se}_x$  and  $\text{V}_2\text{O}_3$  there is a narrow range of the AFM phase that is driven by varying pressure or composition. See, for example, F. Gautier, G. Krill, M. F. Lapiere, P. Panissod, C. Robert, G. Czjzek, J. Fink, and H. Schmidt, *Phys. Lett. A* **53A**, 31 (1975); S. A. Carter, T. F. Rosenbaum, P. Metcalf, J. M. Honig, and J. Spalek, *Phys. Rev. B* **48**, 16 841 (1993).

<sup>9</sup>H. L. Liu, S. L. Cooper, and S.-W. Cheong, *Phys. Rev. Lett.* **81**, 5920 (1998).

<sup>10</sup>T. Katsufuji, *Phys. Rev. B* **51**, 4830 (1995).

- <sup>11</sup>Z. Fang and K. Terakura, Phys. Rev. B **64**, 020509(R) (2001).
- <sup>12</sup>The comprehensive results of uniaxial and hydrostatic pressure studies of  $\text{Ca}_3\text{Ru}_2\text{O}_7$  will be published elsewhere.
- <sup>13</sup>For example, N. Harrison *et al.*, Phys. Rev. B **63**, 081101(R) (2001).
- <sup>14</sup>I. M. Lifshitz and A. M. Kosevich, Sov. Phys. JETP **2**, 636 (1956).
- <sup>15</sup>D. Schoenberg, *Magnetic Oscillations in Metals* (Cambridge University Press, Cambridge, 1984).
- <sup>16</sup>From the amplitude of the SdH oscillations as a function of  $B^{-1}$  one can extract the so-called Dingle temperature,  $T_D = h/4\pi^2 k_B \tau$ , a measure of the purity of samples ( $h$ ,  $k_B$ , and  $\tau$  are the Planck constant, Boltzmann constant, and the relaxation time, respectively) from the Dingle damping factor,  $R_D = \exp(-14.69\mu_c/T_D/B)$ . For the flux-grown  $\text{Ca}_3\text{Ru}_2\text{O}_7$  single crystals studied,  $T_D$  ranges from 1.5 to 3.0 K, which is rare for oxides and comparable to those of good organic metals, whose  $T_D$  varies from 0.5 to 3.5 K. Given such a high quality of the crystals, any unusual electron scattering observed is believed to be intrinsic.
- <sup>17</sup>T. Hotta and E. Dagotto, Phys. Rev. Lett. **88**, 017201 (2001).
- <sup>18</sup>C. S. Alexander, G. Cao, V. Dobrosavljevic, E. Lochner, S. McCall, J. E. Crow, and P. R. Guertin, Phys. Rev. B **60**, R8422 (1999).
- <sup>19</sup>T. Mizokawa, L. H. Tjeng, G. A. Sawatzky, G. Ghiringhelli, O. Tjernberg, N. B. Brookes, H. Fukazawa, S. Nakatsuji, and Y. Maeno, Phys. Rev. Lett. **87**, 077202 (2001).
- <sup>20</sup>E. Dagotto, T. Hotta, and A. Moreo, Phys. Rep. **344**, 1 (2001).
- <sup>21</sup>G. Cao, L. Balicas, Y. Xin, E. Dagotto, J. E. Crow, C. S. Nelson, and D. F. Agterberg, Phys. Rev. B **67**, 060406(R) (2003).
- <sup>22</sup>M. Julliere, Phys. Lett. A **54A**, 225 (1975).
- <sup>23</sup>S. McCall, G. Cao, and J. E. Crow, Phys. Rev. B **67**, 094427 (2003).